Raymo, M.E., Jansen, E., Blum, P., and Herbert, T.D. (Eds.), 1999
Proceedings of the Ocean Drilling Program, Scientific Results, Vol. 162

8. MAGNETIC STRATIGRAPHY OF NORTH ATLANTIC SITES 980–984[1]

J.E.T. Channell[2] and B. Lehman[3]

ABSTRACT

Magnetic polarity stratigraphies for Sites 980–984 are based on shipboard measurements from the pass-through magnetometer after alternating field (AF) demagnetization at a peak field of 25 mT and shore-based stepwise AF demagnetization of discrete samples. The characteristic magnetization component was determined after AF demagnetization removed the steep downward drill-string–related magnetic overprint. Peak AF fields in the 20–30 mT range were required to resolve the component, carried by magnetite, that was used to produce unambiguous Pliocene–Pleistocene magnetic stratigraphies at all five sites. At Sites 980 and 983, magnetic stratigraphies were resolved to the base of the recovered advanced hydraulic piston corer (APC) section, which lies in the Matuyama Chron (1r.2r) and Olduvai Subchron (2n), respectively. At Sites 981 and 982, magnetization intensities decrease sharply in the normal polarity zone corresponding to the Gauss Chron (2An), and magnetic stratigraphies below this level could not be resolved. At Site 984, the resolution of magnetic stratigraphy was curtailed at ~250 meters below seafloor (Olduvai Subchron) by core deformation at the base of the APC section and in the underlying extended core barrel section.

As the magnetic stratigraphies at all four sites are unequivocal, polarity chron interpretations can be made without aid from the biostratigraphy. Mean sedimentation rates within polarity chrons have been calculated and Pliocene–Pleistocene biomagnetostratigraphic correlations tested.

INTRODUCTION AND METHODS

The North Atlantic sites drilled during Ocean Drilling Program (ODP) Leg 162 (Sites 980–984) were located on the Rockall Bank (Site 982), off its southern edge (Sites 980/981), and on the Gardar (Site 983) and Bjorn Drifts (Site 984) (Fig. 1). Archive halves of all core sections were measured on board ship using the cryogenic pass-through magnetometer. The high rate of core recovery at these sites required that cores be processed promptly and, therefore, stepwise alternating field (AF) demagnetization was generally not feasible during the cruise. Most core sections were measured on board ship at a single demagnetization step (generally 25 mT), the choice of peak field being based on stepwise demagnetization of a few core sections and a handful of discrete samples.

Subsequent shore-based discrete sample measurements were necessary to "ground truth" the shipboard magnetic stratigraphy. These samples were collected during the cruise in standard 7-cm^3 plastic boxes and measured at laboratories at Gif-sur-Yvette and at the University of Florida. Natural remanent magnetization was measured before demagnetization and during stepwise AF demagnetization using a peak field increment of 5 mT in the 5–70 mT range, or until the magnetization intensity fell below magnetometer noise level. Orthogonal projections of AF demagnetization data indicated a characteristic magnetization component resolved at peak fields over ~20 mT. A lower coercivity component was observed in most samples, particularly those with a reverse polarity characteristic component. The low-coercivity component is oriented steeply downcore and is probably partly a viscous remanent magnetization imposed by the drill-string assembly and partly a stirred remanent magnetization related to sediment drilling disturbance. The AF range in which the characteristic magnetization component is isolated was picked by eye from orthogonal projections. The direction of the discrete sample characteristic magnetization component was determined using the standard least-squares technique (Kirschvink, 1980). The discrete sample data generally confirmed the shipboard pass-through measurements, but in some cases, notably in the vicinity of the Gauss/Matuyama boundary at Site 981, the shipboard measurements did not isolate the characteristic magnetization component.

SITE 980

Orthogonal projections of progressive AF demagnetization (Fig. 2) of discrete samples from Hole 980A indicated that a characteristic component is well defined in the 20–70 mT AF demagnetization range. Magnetization intensities were reduced to values close to magnetometer noise level after demagnetization at 60–70 mT, indicating the absence of high-coercivity remanence carriers. Characteristic component inclinations from discrete samples (open squares in Fig. 3) are generally consistent with shipboard data from Hole 980A. The positions of polarity chron boundaries indicate that the base of the hole lies in the Matuyama Chron (1r.2r). The Jaramillo Subchron and the Brunhes/Matuyama boundary are well defined. Note that the differences in the values of meters below seafloor (mbsf) corresponding to polarity zone boundaries at the three holes (Fig. 3) are taken into account by the calculation of meters composite depth (Table 1). See Shipboard Scientific Party (1996a) for an explanation of the technique used to calculate composite depths for Leg 162 sites.

SITE 981

Orthogonal projections of AF demagnetization of samples from Hole 981A indicated that a well-defined magnetization component is resolved at peak fields above 20 mT (Fig. 4). For samples from this site, however, magnetization intensities after demagnetization at peak fields of 25 mT decrease sharply at ~150 mbsf (Fig. 5A), close to the Gauss/Matuyama boundary. The decrease in intensity, by almost two orders of magnitude, coincides with the transition from lithostratigraphic Unit I to Unit II. The mean carbonate content of Unit II is 80.1 wt%, whereas Unit I has a mean carbonate content of 44.8 wt% (Shipboard Scientific Party, 1996b). The increase in car-

[1]Raymo, M.E., Jansen, E., Blum, P., and Herbert, T.D. (Eds.), 1999. *Proc. ODP, Sci. Results*, 162: College Station, TX (Ocean Drilling Program).

[2]Department of Geology, University of Florida, Gainesville, FL 32611-2120, U.S.A. jetc@nersp.nerdc.ufl.edu

[3]Laboratoire des Sciences du Climat et de l'Environnement, CNRS-CEA, Avenue de la Terrasse, 91198 Gif-sur-Yvette, France.

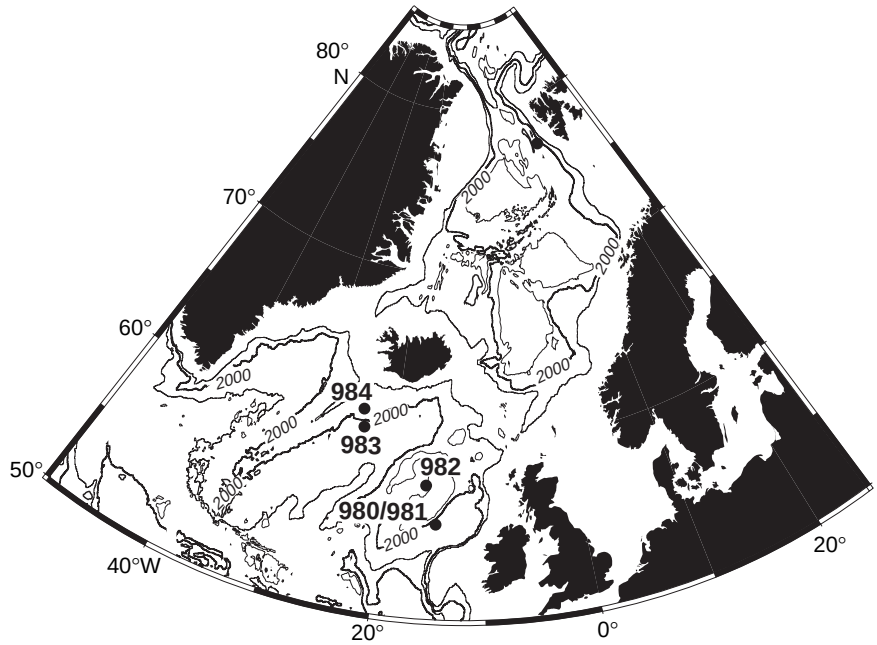

Figure 1. Location map for Sites 980–984. Site 981 lies 2 nmi southeast of Site 980.

bonate content and the accompanying decrease in clay (detrital) content coincides with the drop in magnetization intensity. Shipboard volume susceptibility data indicate a distinct change in concentration of magnetite at the same level (~150 mbsf) (Fig. 6A). The Gauss/Matuyama boundary at Site 981 was placed close to 150 mbsf on the basis of data from the shipboard pass-through magnetometer (Fig. 7). The discrete sample data, however, indicate that this chron boundary is at ~165 mbsf (Table 1, Fig. 7). The weak magnetization intensities and the strong drill-string overprint account for the misidentification of this polarity chron boundary in the shipboard data.

SITE 982

Orthogonal projections of AF demagnetization data for samples from Hole 982B indicate that the characteristic magnetization components are well defined down to ~70 mbsf (Figs. 8, 9). Below this level, magnetization intensities are too low for precise definition of the characteristic component. In the shipboard pass-through data, the decrease in magnetization intensity occurs in the 50–60 mbsf interval (Fig. 5B). As at Site 981, the abrupt decrease in magnetization intensity coincides with the change in carbonate content from mean values of 57.7 to 90.8 wt%, at the boundary between lithostratigraphic Units I and II (Shipboard Scientific Party, 1996c). The concentration of magnetite changes abruptly at the same level, as indicated by the change in multisensor track susceptibility values (Fig. 6B).

SITE 983

The ubiquitous downward magnetic overprint is also present at Site 983; however, it can be eliminated by AF demagnetization at peak fields of 20 mT (Fig. 10). The characteristic magnetization component is particularly well defined at this site, with maximum angular deviation (MAD) values <5°. The base of the recovered section lies within the Olduvai Subchron at Hole 983A and Hole 983B, and just below the Olduvai Subchron at Hole 983C (Fig. 11). Note the presence of one well-defined interval of negative inclinations within the Brunhes Chron in the 15–20 mbsf depth range. This event has an age of 188 ka, occurring close to the oxygen isotopic Stage 6/7 boundary, and has been named the Iceland Basin Event (Channell et al., 1997). The event is included in calculation of sedimentation rates (Table 2). The variable inclination values within the Matuyama Chron may indicate both instability of the geomagnetic field at this time and poorly resolved characteristic magnetization components. Short polarity events (Cobb Mountain and the Gilsa Events) have been recognized between the Jaramillo and the Olduvai Subchrons at Hole 609B (ODP Leg 94) (Clement and Kent, 1987). These events appear to be recorded at Site 983, where sedimentation rates are approximately twice those at Hole 609B. The Cobb Mountain Event is tentatively identified, included in the sedimentation rate calculations (Table 2), and assigned an age of 1.21 Ma (Berggren et al., 1995).

SITE 984

Orthogonal projections of AF demagnetization of samples from this site indicated that a well-defined characteristic magnetization component could be resolved after removal of the steep downward drill-string overprint (Fig. 12). MAD values were usually <10°. The discrete sample component directions from Hole 984B corroborate the shipboard pass-through data (Fig. 13). Below 260 mbsf at Hole 984B, the shipboard pass-through data are compromised by drilling-related deformation at the base of the advanced hydraulic piston corer (APC) section. As at Site 983, the Iceland Basin Event at 188 ka is observed within the Brunhes Chron, and the interval between the Jaramillo and the Olduvai Subchrons appears to be an interval of geomagnetic instability. The Cobb Mountain Event is tentatively identified below the Jaramillo Subchron and is included in the interval sedimentation rate calculations (Table 2).

SEDIMENTATION RATES AND BIOSTRATIGRAPHIC CORRELATIONS

Before Leg 162, conventional piston cores had shown that the sedimentation rates were high in the uppermost ~15 m on the Feni, Gardar, and Bjorn Drifts. It was not known, however, whether these high sedimentation rates continued at depth or whether the drift deposition was interrupted by unconformities. From the magnetic stratigraphy, sedimentation rates within the Brunhes Chron are comparable at Feni (Site 980), Gardar (Site 983), and Bjorn (Site 984) (Fig. 14;

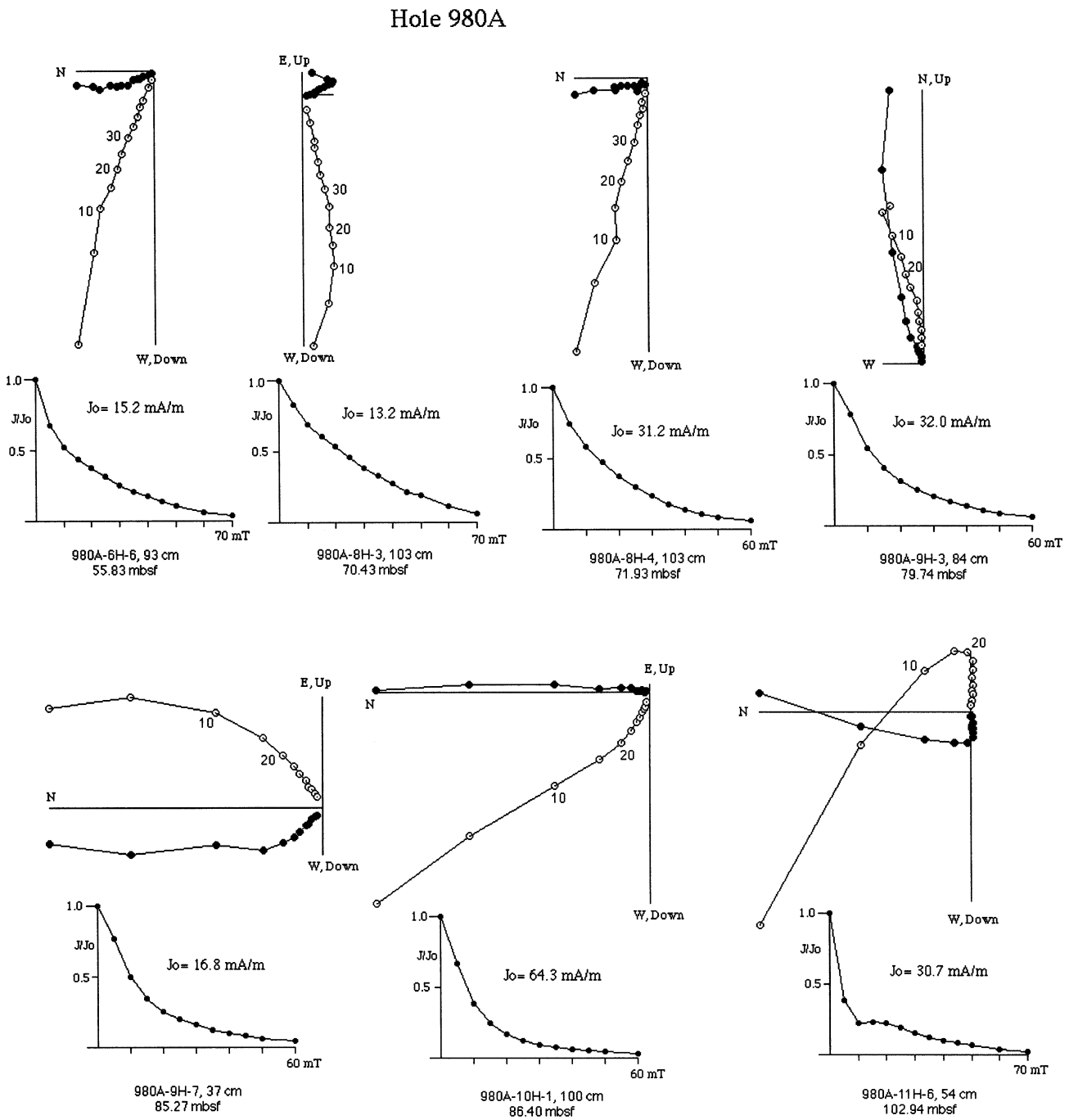

Figure 2. Orthogonal projection of AF demagnetization data from discrete samples in the 50–110 mbsf interval of Hole 980A. Open and solid symbols indicate projections on the vertical and horizontal planes, respectively. J_0 = magnetization intensity before demagnetization.

Table 2). At the second site on the Feni Drift (Site 981), Brunhes sedimentation rates are lower than at Site 980. This was expected from the seismic stratigraphy linking Sites 980 and 981. The upper Pleistocene deposits are seen to thicken toward Site 980, and the Pliocene–lower Pleistocene deposits thicken toward Site 981 (Shipboard Scientific Party, 1996b). The lack of data in the lower parts of the sections at Sites 981 and 982 (Fig. 14) was caused by decreasing magnetization intensities at ~150 and 60 mbsf, respectively, at these two sites (Fig. 5). The lack of data at the base of the section at Site 984 (Fig. 14) resulted from core deformation at the base of the APC section.

In the intervals for which we have magnetostratigraphic control, no abrupt changes in sedimentation rates are apparent (Fig. 15). As expected from the seismic stratigraphy, sedimentation rates at Site 980 decrease with depth and those at Site 981 increase with depth. At the top of the section, Site 984 sedimentation rates are high relative to those at Site 983; however, the converse is true in the lower part of the two magnetostratigraphic sections (Fig. 15; Table 2). All sites that record the Reunion Event at 2.14–2.15 Ma, particularly Site 981, show a step in the age-depth curve. This may indicate a problem with the duration of the Reunion Event (10 k.y.) in the time scale used (Cande and Kent, 1995). At Sites 981, 982, and 984, the Reunion

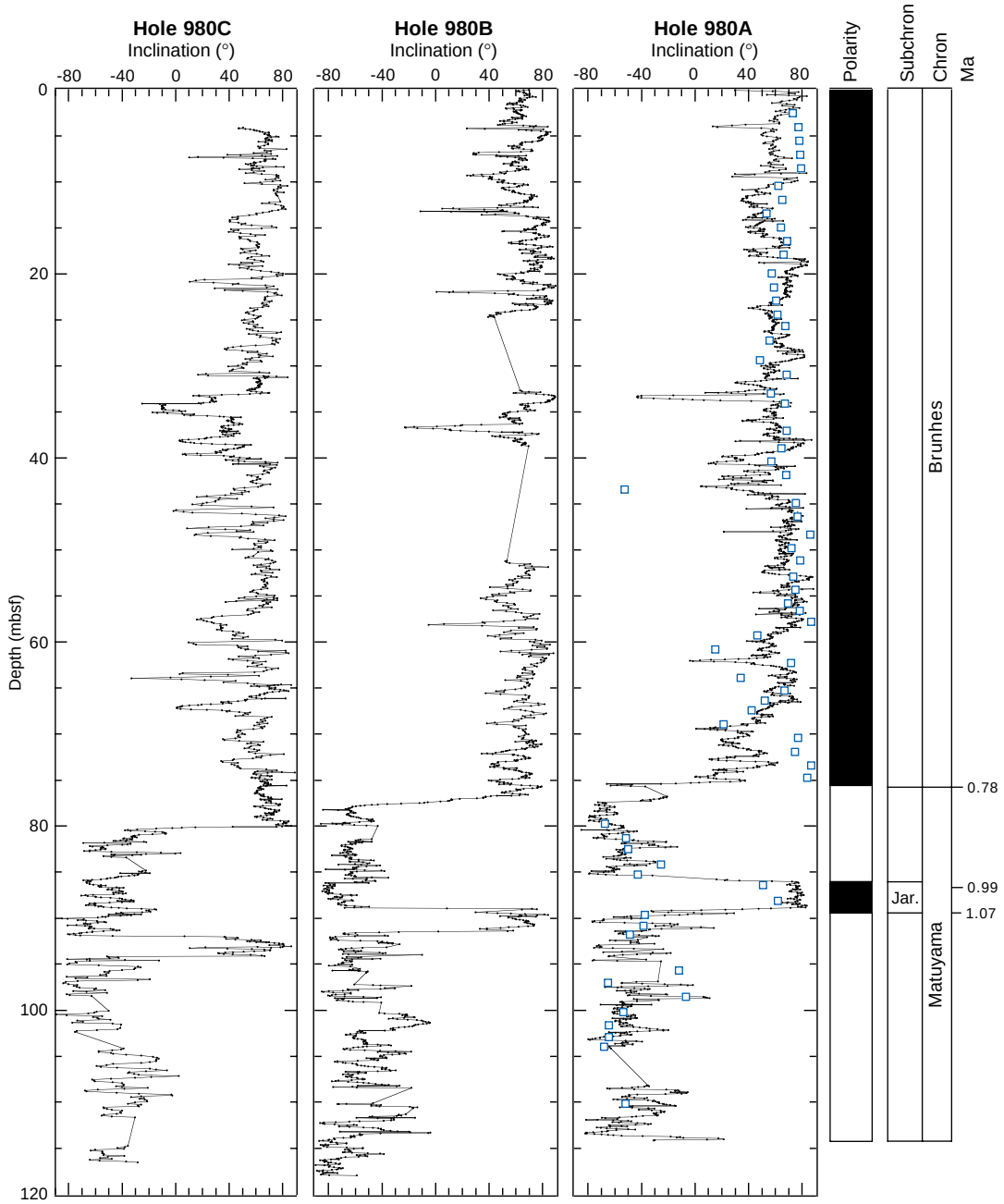

Figure 3. Shipboard (pass-through magnetometer) inclination data after AF demagnetization at peak fields of 25 mT for Site 980 in the 0–120 mbsf interval. Open squares indicate component inclinations determined from discrete (7 cm^3) samples measured postcruise. Component directions were computed from orthogonal projections of AF demagnetization data. Jar. = Jaramillo.

Event is inexplicably expanded on this time scale. The Cande and Kent (1992) time scale assigned a duration of 32 k.y. to the Reunion Subchron, which results in more uniform sedimentation rates in the vicinity of the Reunion Subchron at both Sites 983 and 984 (Table 2).

The quality of the magnetic stratigraphies at Sites 980–984 is such that magnetostratigraphic (polarity chron) interpretations can be made without the guidance of biostratigraphic datums. For this reason, Sites 980–984 provide a useful reference for late Pliocene–Pleistocene biomagnetostratigraphic correlations. The superposition (ordering) of biostratigraphic events is generally consistent among the four sites (Fig. 16); however, the correlations of biostratigraphic events with polarity chrons show some variations. For example, the *Gephyrocapsa* spp. events occur between the Olduvai Subchron and just above the Brunhes/Matuyama boundary. The exact positions of each of these events vary, however, from site to site (Fig. 16). Assuming uniform sedimentation rate within polarity chrons, we have calculated the age of well-defined biostratigraphic events and compared these ages with the compilation of Berggren et al. (1995) (Table 3). Although the site with the lowest sedimentation rates (Site 982) yields the more inconsistent ages of bioevents, these ages are generally consistent with the Berggren et al. (1995) compilation.

ACKNOWLEDGMENTS

We thank C. Kissel and C. Laj for logistical support, K. Huang for laboratory assistance, and B. Clement and G. Muttoni for reviews of the manuscript. The paleomagnetic laboratory at Gif-sur-Yvette is

Table 1. Position of polarity chron boundaries at Sites 980–984.

	Hole 980A mbsf (mcd)	Hole 980B mbsf (mcd)	Hole 980C mbsf (mcd)	Hole 981A mbsf (mcd)	Hole 981B mbsf (mcd)	Hole 982A mbsf (mcd)	Hole 982B mbsf (mcd)	Hole 982C mbsf (mcd)
Brunhes/Matuyama (0.78 Ma)	75.25 (87.56)	77.35 (87.05)	80.20 (87.35)*	49.17 (54.69)	48.00 (54.76)*		17.50 (19.66)*	20.10 (20.08)
Top Jaramillo (0.99 Ma)	85.60 (99.83)	88.95 (100.38)	92.00 (100.33)*	58.47 (65.57)	58.15 (65.59)		23.35 (25.51)	24.30 (27.82)
Base Jaramillo (1.07 Ma)	89.20 (103.43)*	91.45 (103.74)	94.12 (103.71)	61.55 (68.65)	60.22 (69.49)	28.15 (30.65)	24.97 (28.05)*	25.25 (28.77)
Cobb Mt. Event (1.21 Ma)				67.65 (75.45)	66.45 (75.72)			
Top Olduvai (1.77 Ma)				96.77 (108.33)*	96.80 (107.10)		36.15 (40.23)*	36.82 (40.08)
Base Olduvai (1.95 Ma)				107.50 (119.60)	109.60 (120.75)*	39.45 (43.38)	39.17 (43.25)*	40.45 (43.71)
Top Reunion (2.14 Ma)				120.17 (133.53)	123.60 (135.02)*	43.30 (47.23)	43.12 (47.20)	41.80 (46.38)*
Base Reunion (2.15 Ma)				124.27 (138.29)*	125.25 (136.67)	43.57 (47.50)	43.50 (49.01)	43.25 (47.83)*
Matuyama/Gauss (2.58 Ma)				165.00 (180.78)	163.80 (178.08)*	50.70 (57.23)	52.55 (58.06)*	50.93 (55.51)

Note: * = within composite section.

Table 1 (continued).

	Hole 983A mbsf (mcd)	Hole 983B mbsf (mcd)	Hole 983C mbsf (mcd)	Hole 984A mbsf (mcd)	Hole 984B mbsf (mcd)	Hole 984C mbsf (mcd)	Hole 984D mbsf (mcd)
Iceland Basin Event (188 ka)	17.85 (20.51)	18.80 (20.69)	15.50 (20.74)*	29.00 (31.54)	26.85 (29.92)	27.05 (31.52)*	
Brunhes/Matuyama (0.78 Ma)	81.97 (90.82)	82.70 (90.76)*	79.15 (90.57)	97.40 (107.52)	100.20 (108.06)	96.67 (107.51)*	
Top Jaramillo (0.99 Ma)	106.35 (117.17)	107.30 (117.07)	103.90 (117.23)*	119.30 (130.54)	121.70 (131.97)*	120.70 (131.72)	
Base Jaramillo (1.07 Ma)	119.40 (131.01)	120.17 (131.83)*	118.20 (132.63)	131.65 (144.78)	132.47 (144.65)	132.40 (144.84)*	
Cobb Mt. Event (1.21 Ma)	136.75 (149.56)	136.50 (148.95)	134.50 (149.82)*	139.70 (153.55)	140.72 (152.90)	140.80 (153.24)*	
Top Olduvai (1.77 Ma)	225.40 (247.36)	225.20 (246.93)*	222.60 (246.48)		195.90 (214.30)	196.90 (214.78)	196.80 (214.15)*
Base Olduvai (1.95 Ma)			254.80 (281.95)*		217.10 (237.18)	217.25 (237.09)	216.60 (237.07)*
Top Reunion (2.14 Ma)					241.80 (264.39)	241.00 (264.03)	240.20 (263.62)*
Base Reunion (2.15 Ma)					245.50 (268.09)*	244.37 (267.40)	242.90 (266.83)

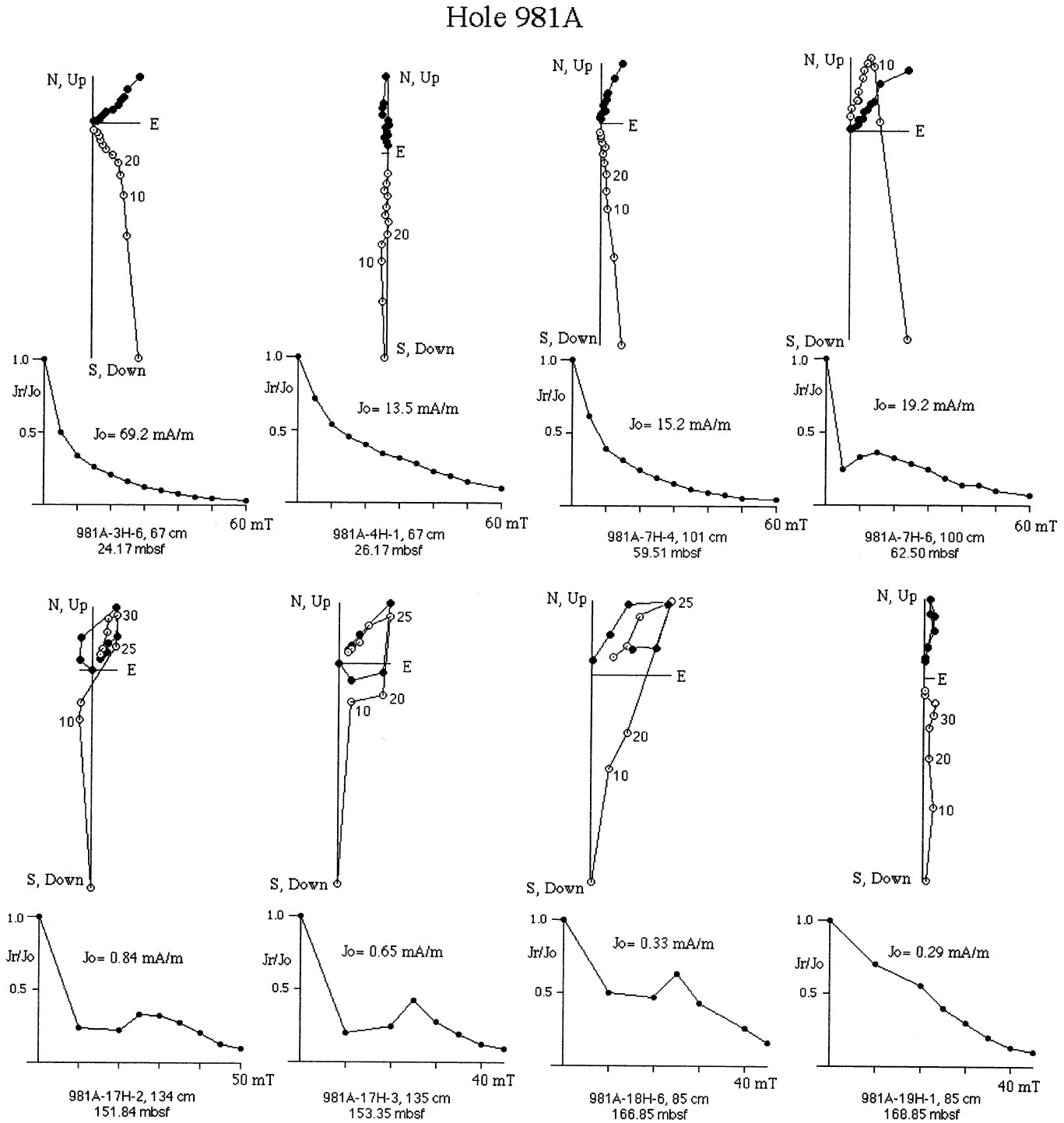

Figure 4. Orthogonal projection of AF demagnetization data from discrete samples in the 20–170 mbsf interval of Hole 981A. Open and solid symbols indicate projections on the vertical and horizontal planes, respectively. J_0 = magnetization intensity before demagnetization.

supported by CEA and CNRS. At the University of Florida, this project was supported by the U.S. Science Support Program, LSCE contribution number 35.

REFERENCES

Berggren, W.A., Hilgen, F.J., Langereis, C.G., Kent, D.V., Obradovich, J.D., Raffi, I., Raymo, M.E., and Shackleton, N.J., 1995. Late Neogene chronology: new perspectives in high-resolution stratigraphy. *Geol. Soc. Am. Bull.*, 107:1272–1287.

Cande, S.C., and Kent, D.V., 1992. A new geomagnetic polarity time scale for the Late Cretaceous and Cenozoic. *J. Geophys. Res.*, 97:13917–13951.

Cande, S.C., and Kent, D.V., 1995. Revised calibration of the geomagnetic polarity timescale for the Late Cretaceous and Cenozoic. *J. Geophys. Res.*, 100:6093–6095.

Channell, J.E.T., Hodell, D.A., and Lehman, B., 1997. Relative geomagnetic paleointensity and $\delta^{18}O$ at ODP Site 983 (Gardar Drift, North Atlantic) since 350 ka. Earth Planet. Sci. Lett., 153: 103–118.

Clement, B.M., and Kent, D.V., 1987. Short polarity intervals within the Matuyama: transitional field records from hydraulic piston core sites from the North Atlantic. *Earth Planet. Sci. Lett.*, 81:253–264.

Jansen, E., Raymo, M.E., Blum, P., et al., 1996. *Proc. ODP, Init. Repts.*, 162: College Station, TX (Ocean Drilling Program).

Kirschvink, J.L., 1980. The least-squares line and plane and the analysis of palaeomagnetic data. *Geophys. J. R. Astron. Soc.*, 62:699–718.

Shipboard Scientific Party, 1996a. Explanatory notes. *In* Jansen, E., Raymo, M.E., Blum, P., et al., *Proc. ODP, Init. Repts.*, 162: College Station, TX (Ocean Drilling Program), 21–45.

Shipboard Scientific Party, 1996b. Sites 980/981. *In* Jansen, E., Raymo, M.E., Blum, P., et al., *Proc. ODP, Init. Repts.*, 162: College Station, TX (Ocean Drilling Program), 49–90.

Shipboard Scientific Party, 1996c. Site 982. *In* Jansen, E., Raymo, M.E., Blum, P., et al., *Proc. ODP, Init. Repts.*, 162: College Station, TX (Ocean Drilling Program), 91–138.

Date of initial receipt: 10 September 1997
Date of acceptance: 11 June 1998
Ms 162SR-002

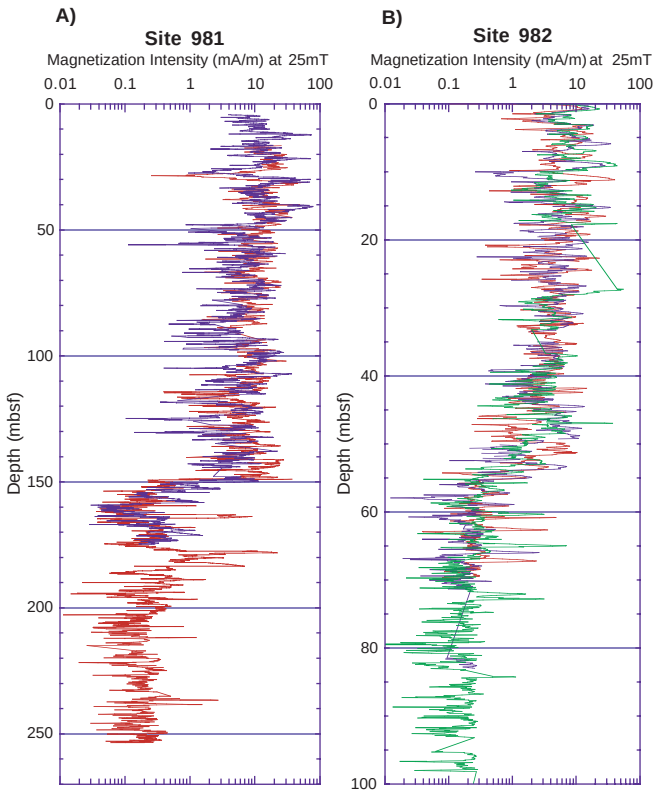

Figure 5. Magnetization intensities (after AF demagnetization at peak fields of 25 mT) of archive core halves from the shipboard pass-through magnetometer for **(A)** Holes 981A and 981B combined and **(B)** Holes 982A, 982B, and 982C combined.

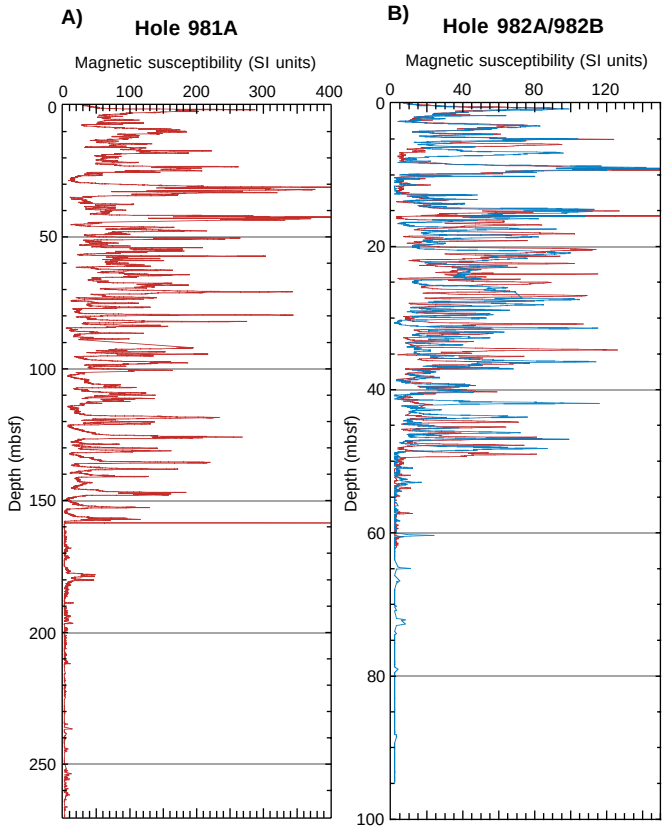

Figure 6. Volume susceptibility from the shipboard multisensor track. **A.** Hole 981A. **B.** Holes 982A and 982B.

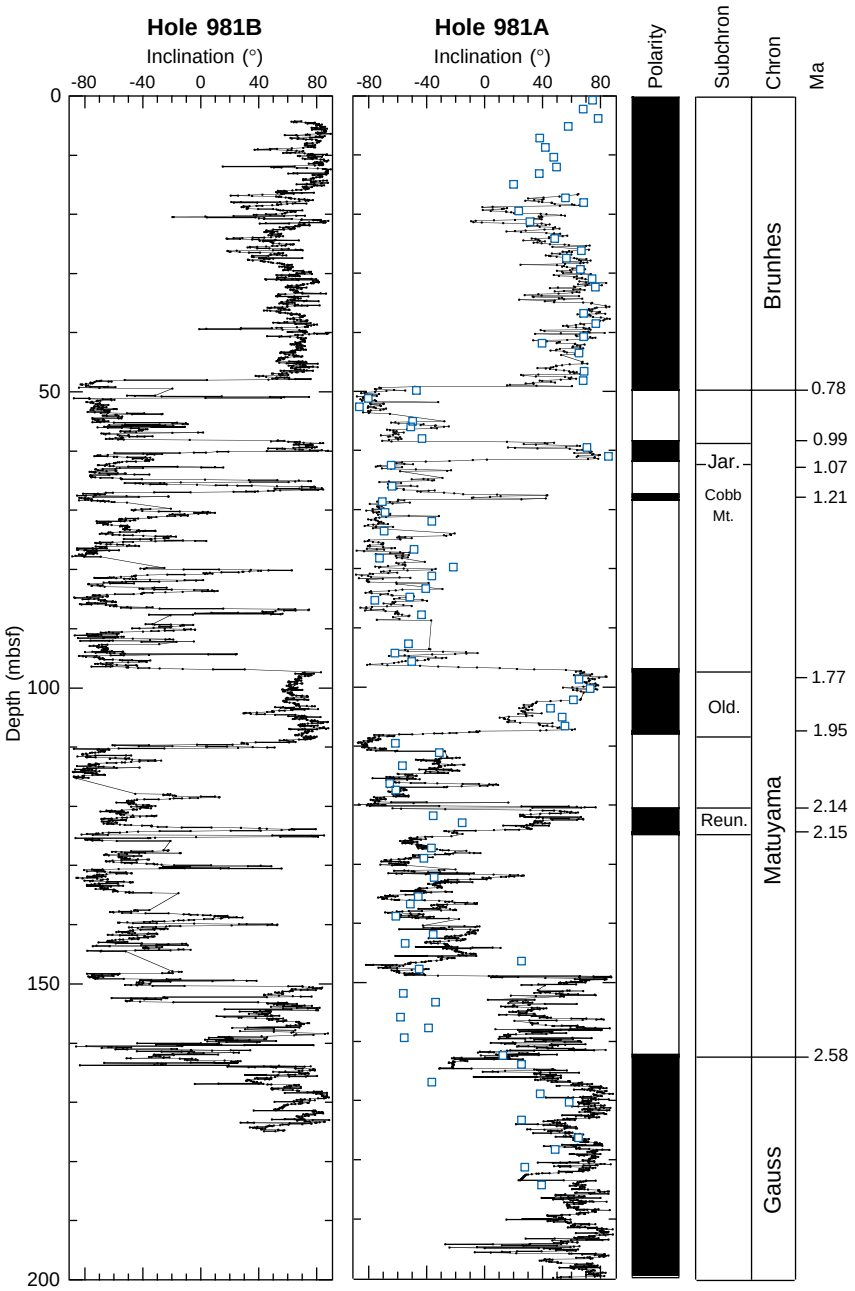

Figure 7. Shipboard (pass-through magnetometer) inclination data after AF demagnetization at peak fields of 25 mT for Site 981 in the 0–200 mbsf interval. Open squares indicate component inclinations determined from discrete (7 cm^3) samples measured postcruise. Component directions were computed from orthogonal projections of AF demagnetization data. Jar. = Jaramillo, Reun. = Reunion, Old. = Olduvai.

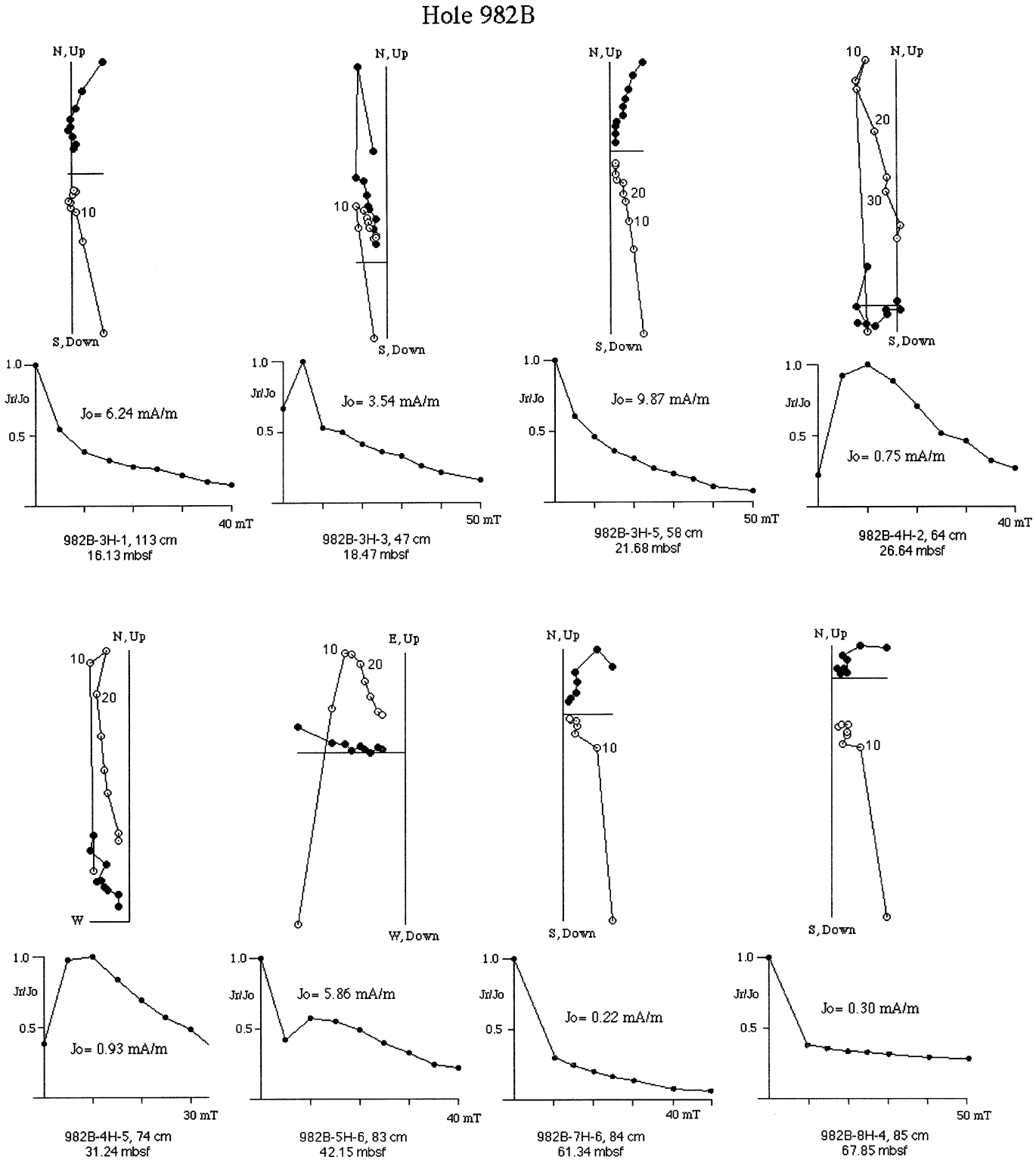

Figure 8. Orthogonal projection of AF demagnetization data from discrete samples in the 15–70 mbsf interval of Hole 982B. Open and solid symbols indicate projection on the vertical and horizontal planes, respectively. Other symbols as for Figure 2.

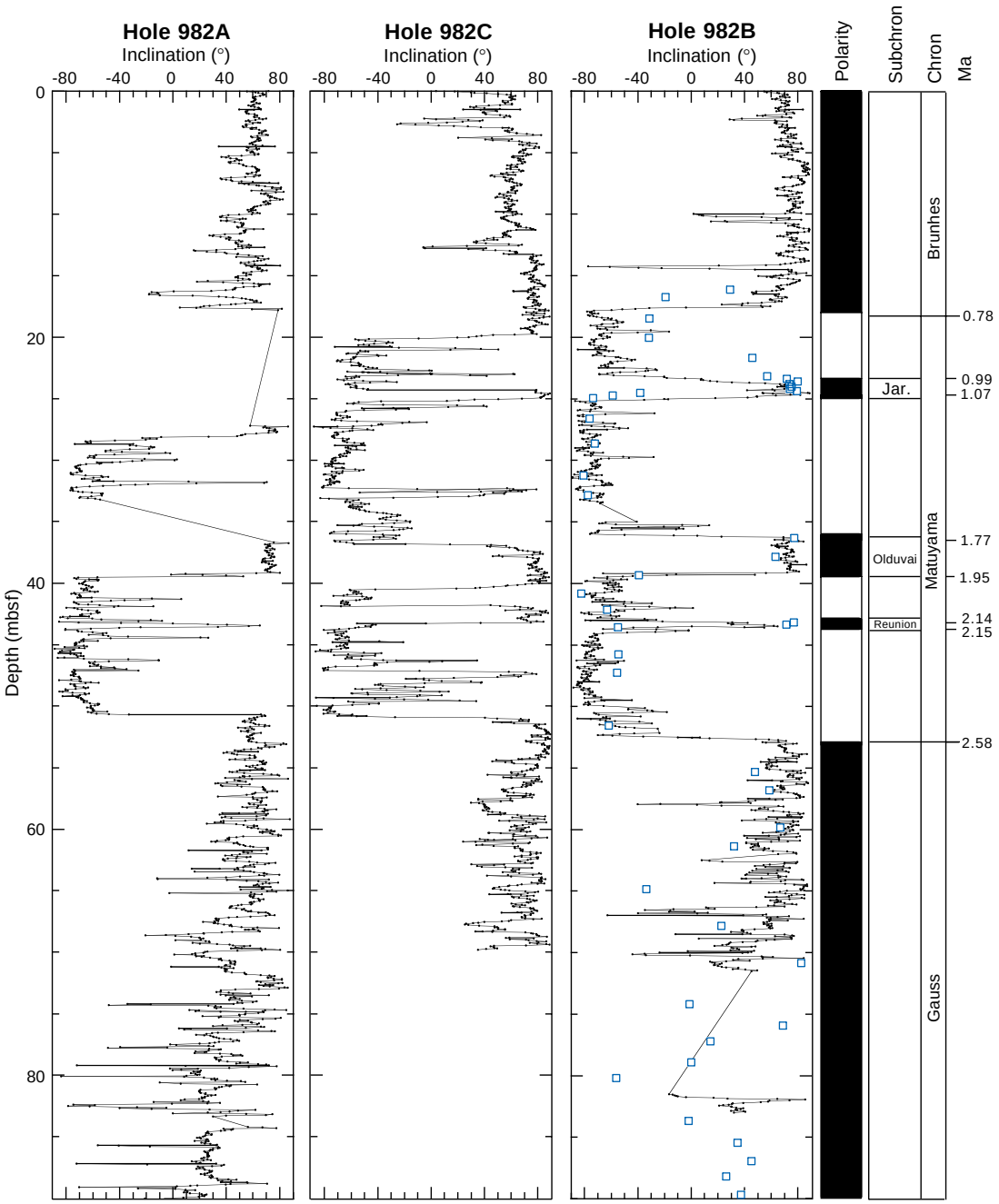

Figure 9. Shipboard (pass-through magnetometer) inclination data after AF demagnetization at peak fields of 25 mT for Site 982 in the 0–90 mbsf interval. Open squares indicate component inclinations determined from discrete (7 cm^3) samples measured postcruise. Component directions were computed from orthogonal projections of AF demagnetization data. Jar. = Jaramillo.

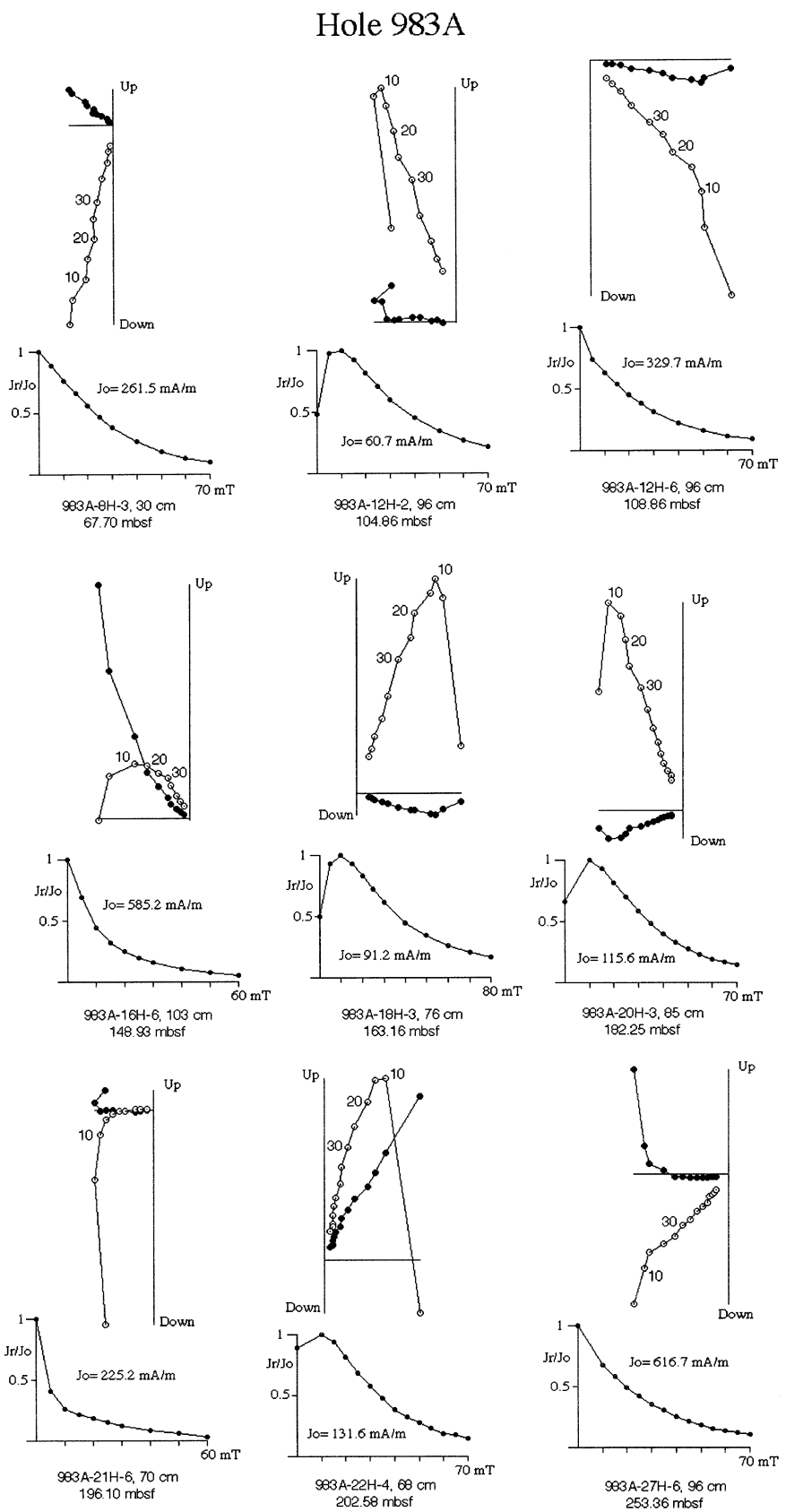

Figure 10. Orthogonal projection of AF demagnetization data from discrete samples in the 60–260 mbsf interval of Hole 983A. Open and solid symbols indicate projection on the vertical and horizontal planes, respectively. Other symbols as for Figure 2.

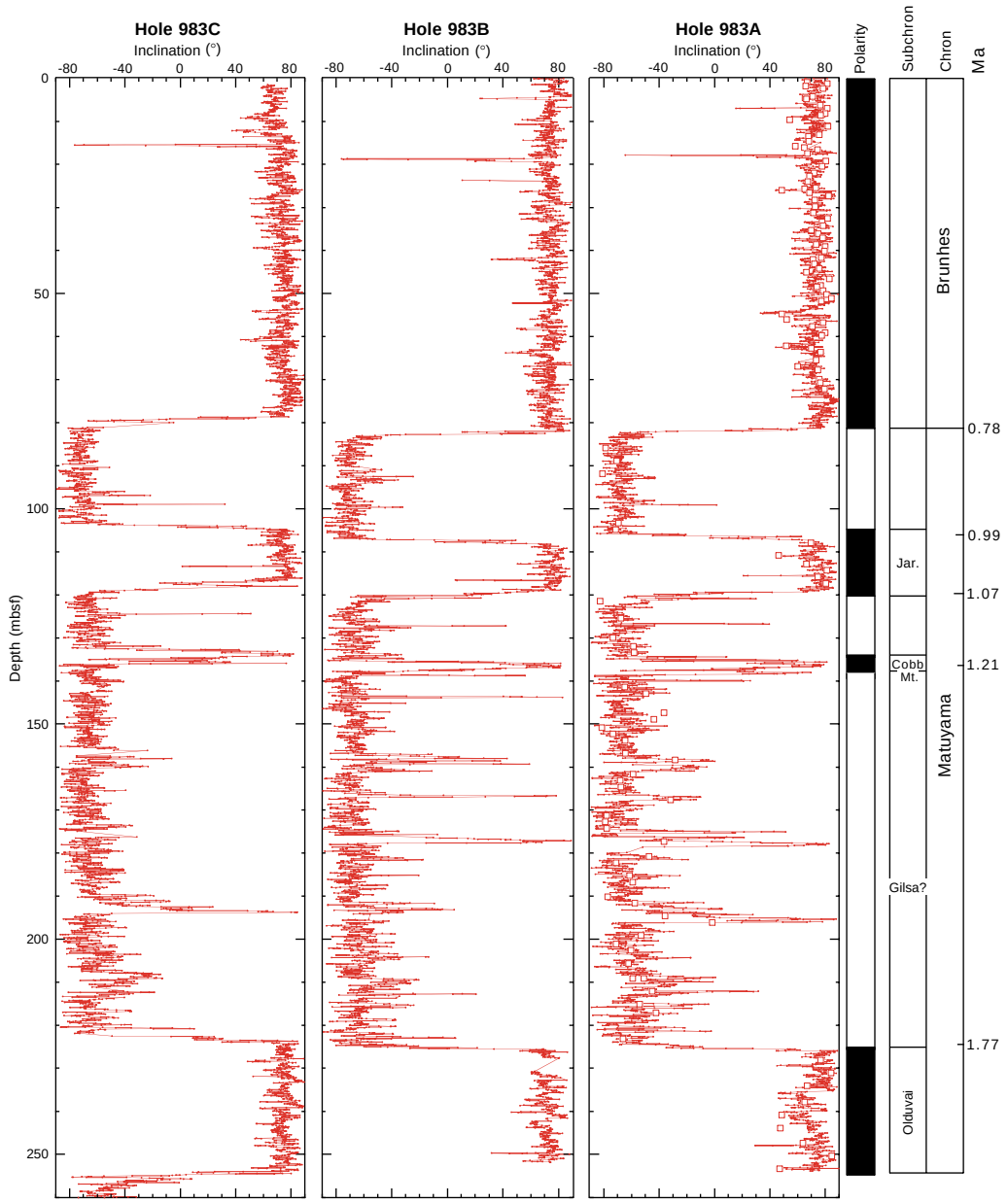

Figure 11. Shipboard (pass-through magnetometer) inclination data after AF demagnetization at peak fields of 25 mT for Site 983 in the 0–260 mbsf interval. Open squares indicate component inclinations determined from discrete (7 cm^3) samples measured postcruise. Component directions computed from orthogonal projections of AF demagnetization data. Jar. = Jaramillo.

Table 2. Interval mean sedimentation rates for Sites 980–984.

Event (age)	Hole 980A mbsf/m.y. (mcd/m.y.)	Hole 980B mbsf/m.y. (mcd/m.y.)	Hole 980C mbsf/m.y. (mcd/m.y.)	Hole 981A mbsf/m.y. (mcd/m.y.)	Hole 981B mbsf/m.y. (mcd/m.y.)	Hole 982A mbsf/m.y. (mcd/m.y.)	Hole 982B mbsf/m.y. (mcd/m.y.)	Hole 982C mbsf/m.y. (mcd/m.y.)
Core top (0)								
	96.47 (112.26)	99.17 (111.60)	102.82 (111.99)	63.04 (70.12)	61.54 (70.21)		22.44 (25.21)	25.77 (25.74)
Brunhes/Matuyama (0.78 Ma)								
	49.29 (58.43)	55.24 (63.48)	56.19 (61.81)	44.29 (51.81)	48.33 (51.57)		27.86 (27.86)	20.00 (36.86)
Top Jaramillo (0.99 Ma)								
	45.00 (45.00)	31.25 (42.00)	26.50 (41.75)	38.50 (38.50)	25.86 (48.75)		20.25 (31.75)	11.88 (11.88)
Base Jaramillo (1.07 Ma)								
				43.57 (48.57)	44.50 (44.50)			
Cobb Mt. Event (1.21 Ma)								
				52.00 (58.72)	54.20 (56.04)			
Top Olduvai (1.77 Ma)								
				59.61 (62.61)	71.11 (75.56)		16.78 (16.78)	20.17 (20.17)
Base Olduvai (1.95 Ma)								
				66.68 (73.32)	73.68 (75.37)	20.26 (20.26)	20.79 (20.79)	7.11 (14.05)
Top Reunion (2.14 Ma)								
				410 (476) 128.13 (148.75)*	165 (165) 51.56 (51.56)*	270 (270) 8.44 (8.44)*	380 (181) 11.87 (56.56)*	145 (145) 45.31 (45.31)*
Base Reunion (2.15 Ma)								
				94.72 (98.81)	89.65 (96.30)	16.58 (22.63)	21.05 (21.05)	17.86 (17.86)
Matuyama/Gauss (2.58 Ma)								

Notes: Polarity chron boundary ages from Cande and Kent (1995). Result marked with asterisk uses alternative duration of Reunion Event (0.032 m.y.) from Cande and Kent (1992).

Table 2 (continued).

Event (age)	Hole 983A mbsf/m.y. (mcd/m.y.)	Hole 983B mbsf/m.y. (mcd/m.y.)	Hole 983C mbsf/m.y. (mcd/m.y.)	Hole 984A mbsf/m.y. (mcd/m.y.)	Hole 984B mbsf/m.y. (mcd/m.y.)	Hole 984C mbsf/m.y. (mcd/m.y.)	Hole 984D mbsf/m.y. (mcd/m.y.)
Core top (0)							
	95.97 (110.27)	101.08 (111.24)	83.33 (111.51)	155.91 (169.57)	144.35 (160.86)	145.43 (169.46)	
Iceland Basin Event (188 ka)							
	107.95 (118.37)	107.58 (117.96)	107.15 (117.56)	115.15 (127.91)	123.48 (131.55)	117.21 (127.93)	
Brunhes/Matuyama (0.78 Ma)							
	116.10 (125.48)	117.14 (125.30)	117.86 (126.95)	104.29 (109.14)	102.38 (113.86)	114.43 (115.29)	
Top Jaramillo (0.99 Ma)							
	163.13 (173.00)	160.88 (184.50)	178.75 (185.13)	154.38 (179.25)	134.63 (158.50)	146.25 (164.00)	
Base Jaramillo (1.07 Ma)							
	123.93 (132.50)	116.64 (122.29)	116.43 (127.00)	57.50 (58.93)	58.93 (58.93)	60.00 (60.00)	
Cobb Mt. Event (1.21 Ma)							
	158.30 (174.64)	158.39 (174.96)	157.32 (172.61)		98.54 (109.64)	100.18 (109.89)	
Top Olduvai (1.77 Ma)							
			178.89 (197.06)		117.78 (127.11)	113.06 (123.94)	110.00 (128.44)
Base Olduvai (1.95 Ma)							
					130.00 (143.21)	125.00 (141.79)	124.21 (138.68)
Top Reunion (2.14 Ma)							
					370 (370) 115.63 (115.63)	337 (337) 105.31 (105.31)*	270 (321) 84.38 (100.31)*
Base Reunion (2.15 Ma)							

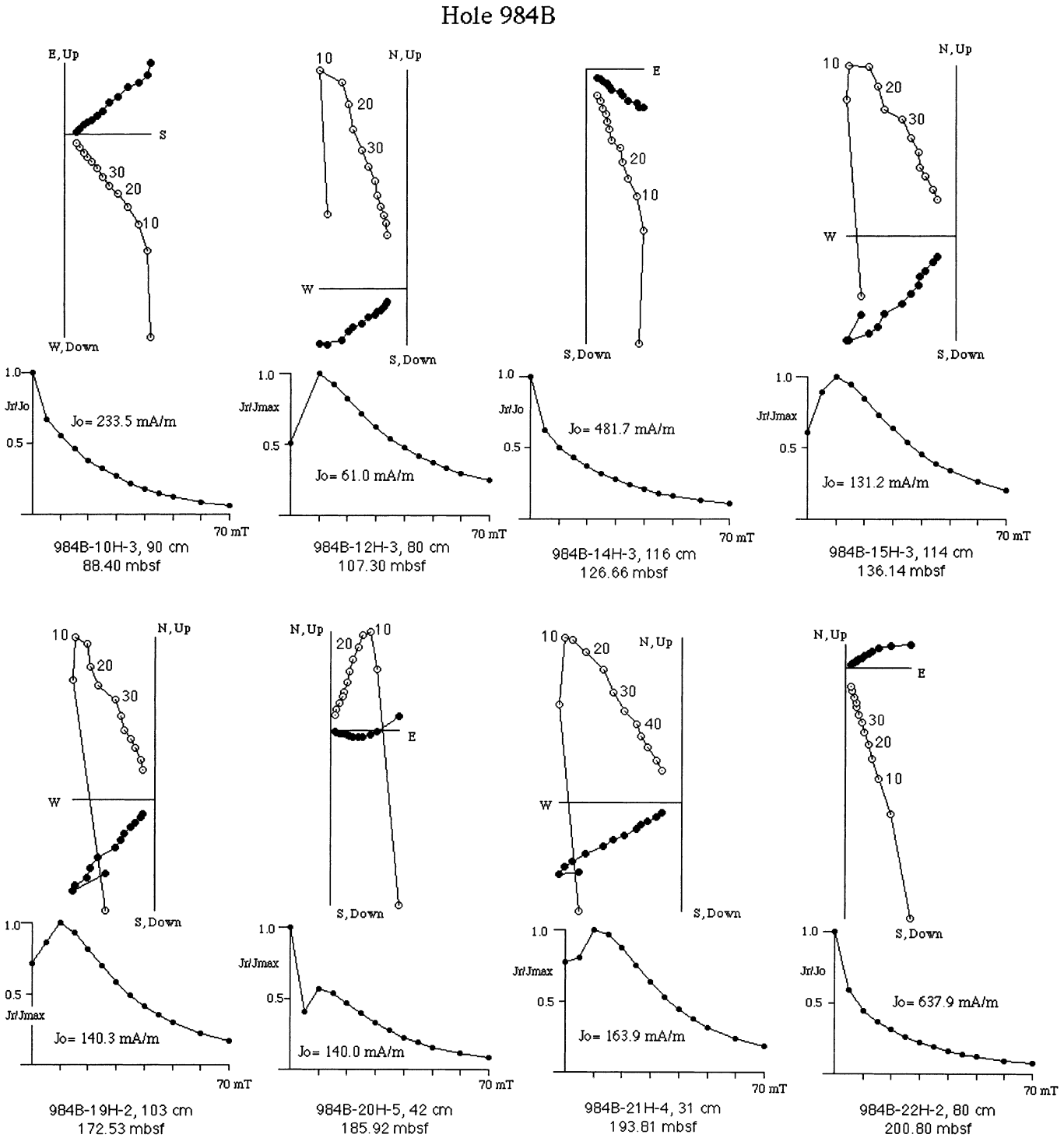

Figure 12. Orthogonal projection of AF demagnetization data from discrete samples in the 80–210 mbsf interval of Hole 984B. Open and solid symbols indicate projection on the vertical and horizontal planes, respectively. Other symbols as for Figure 2.

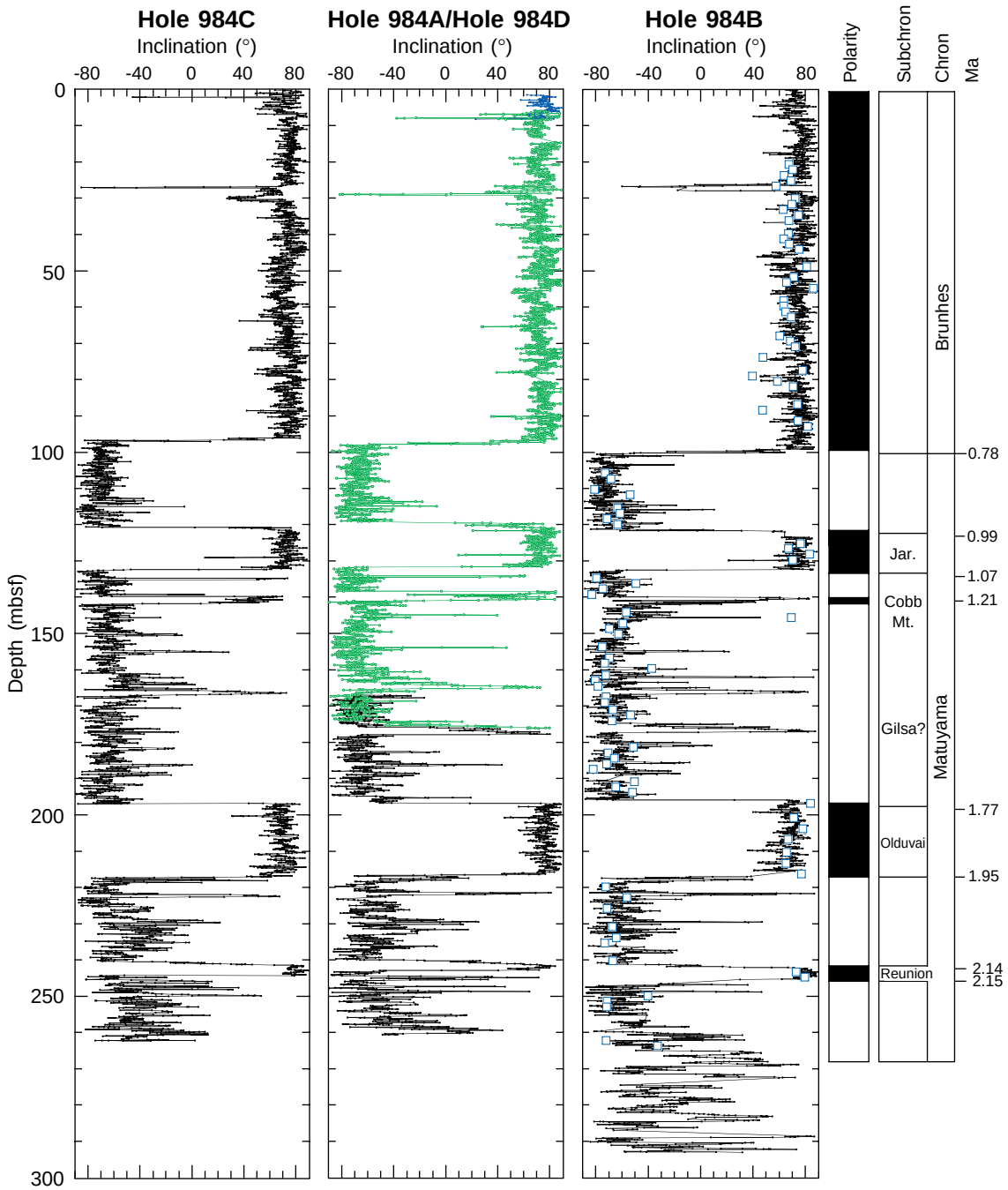

Figure 13. Shipboard (pass-through magnetometer) inclination data after AF demagnetization at peak fields of 25 mT for Site 984 in the 0–300 mbsf interval. Open squares indicate component inclinations determined from discrete (7 cm^3) samples measured postcruise. Component directions were computed from orthogonal projections of AF demagnetization data. The Hole 984A and Hole 984D shipboard data are superimposed. The 0–176 mbsf interval was recovered from Hole 984A, and the 0–8 and 166–270 mbsf intervals were recovered from Hole 984D. Jar. = Jaramillo.

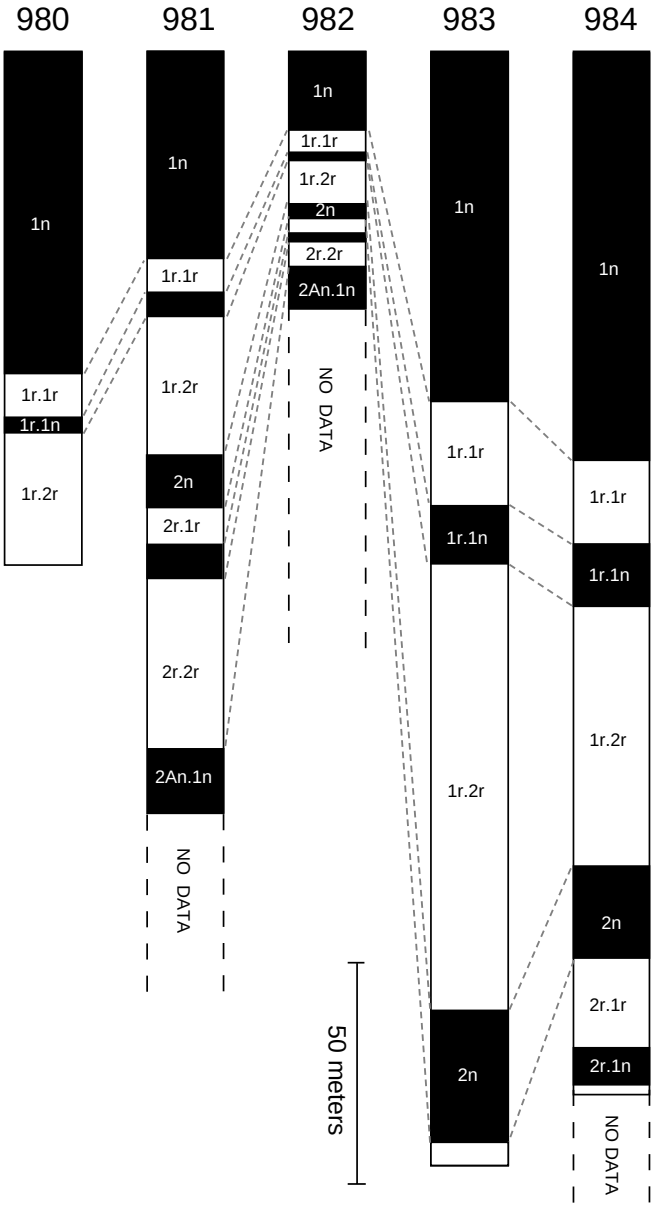

Figure 14. Magnetic polarity stratigraphies from Sites 980 to 984 on a uniform vertical (depth) scale. Polarity chron nomenclature from Cande and Kent (1992).

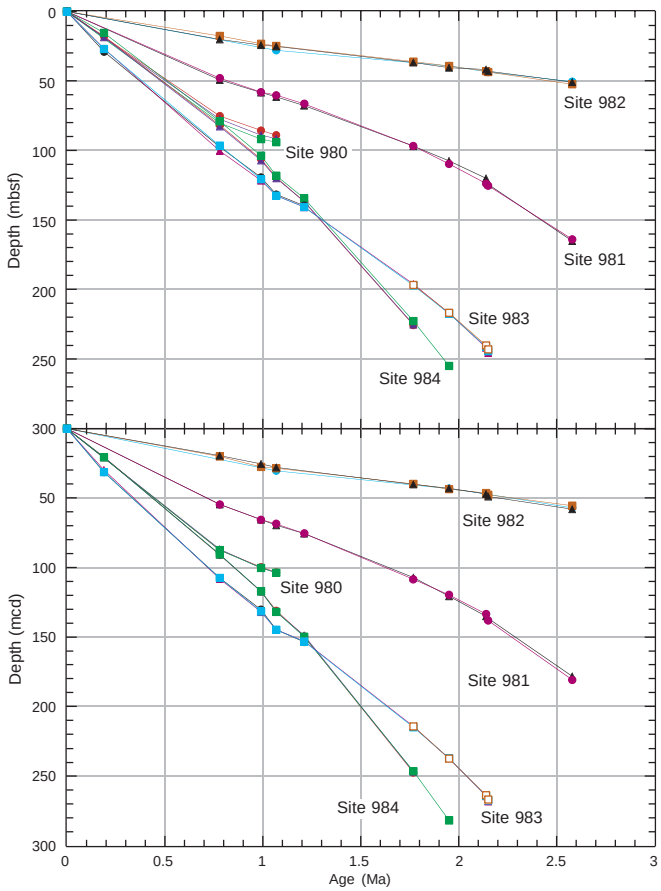

Figure 15. Age-depth plots based on magnetostratigraphic interpretations for individual holes from each site. Top = meters below seafloor, base = meters composite depth.

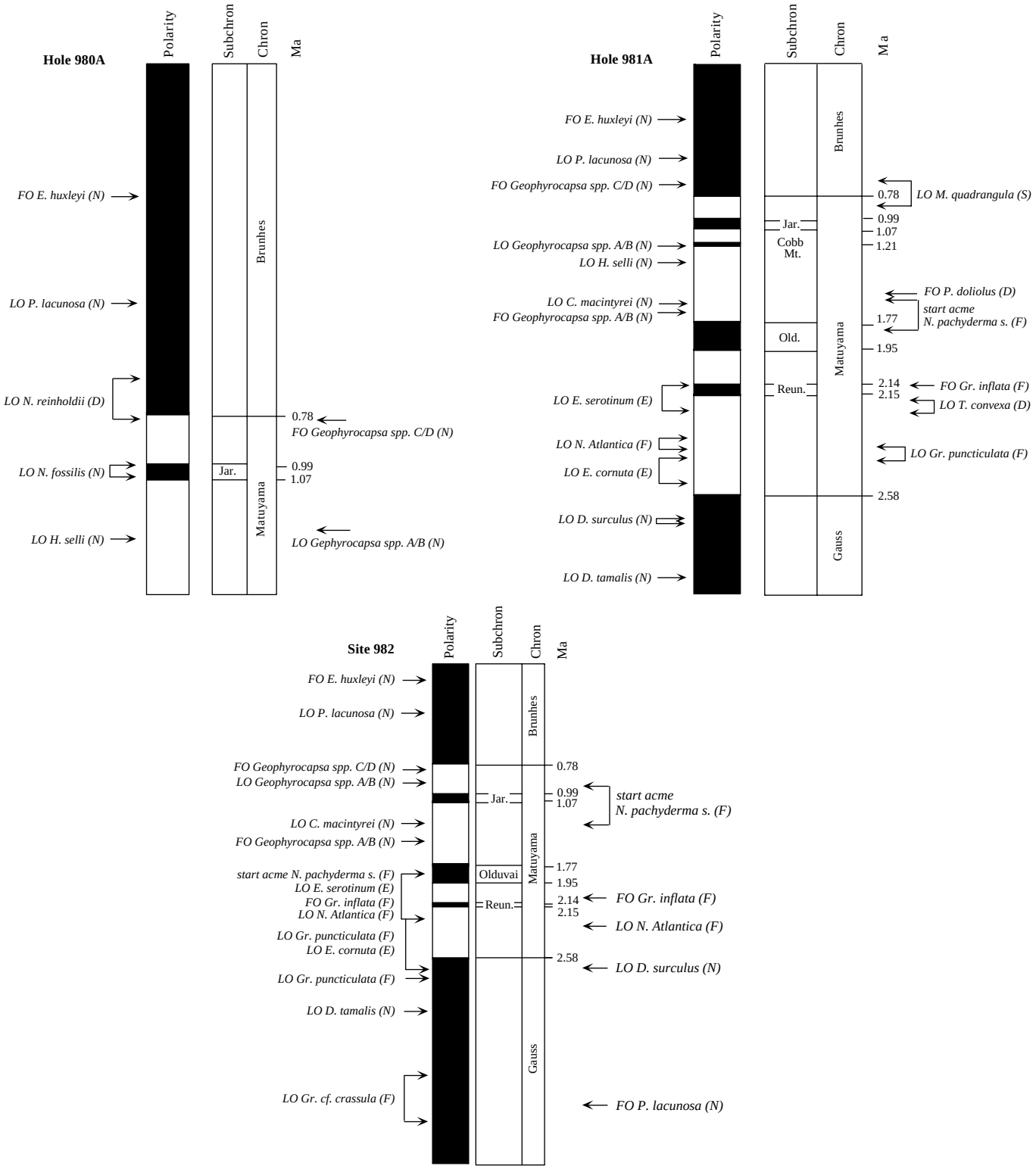

Figure 16. Correlation of biostratigraphic markers with polarity chrons. FO = first occurrence, LO = last occurrence, N = calcareous nannofossil event, F = planktonic foraminifer event, D = diatom event, S = silicoflagellate event, E = ebridan event. Other abbreviations as in Figure 7. At Sites 982 and 984, multiple observations from different holes are indicated. Biostratigraphic data are from Jansen, Raymo, Blum, et al. (1996) compilation. (Continued on next page.)

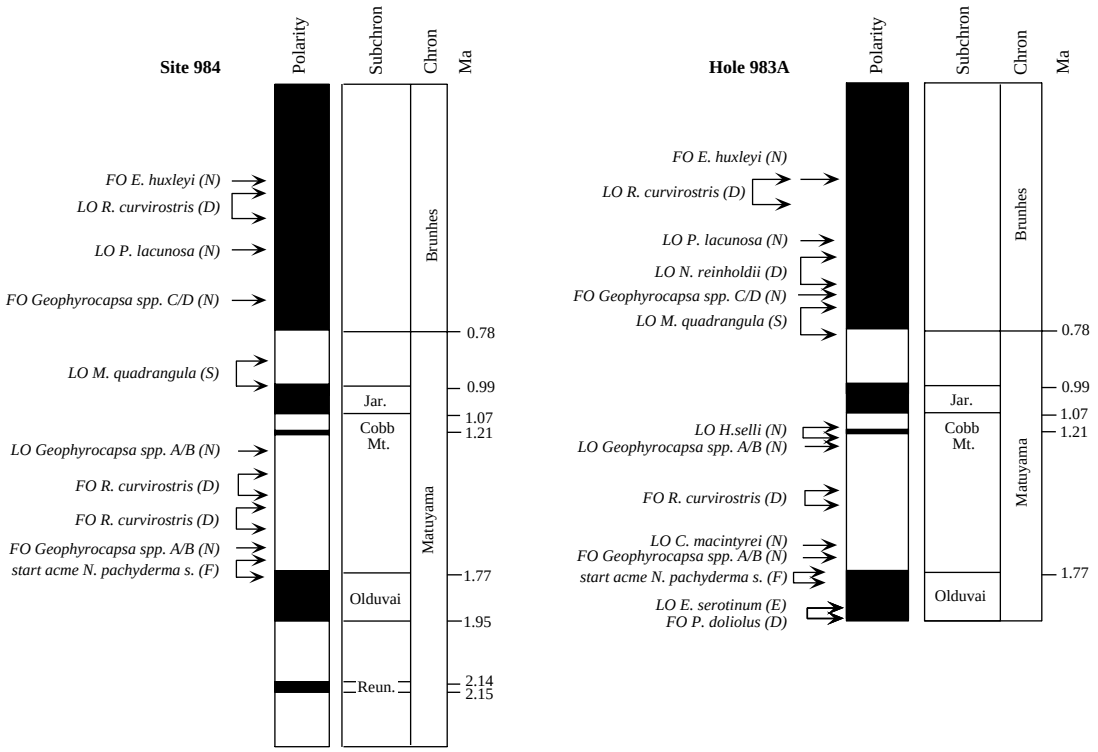

Figure 16 (continued).

Table 3. Age (Ma) of biostratigraphic events, assuming uniform sedimentation rates within polarity chrons at Sites 980–984 and comparison with ages given in the Berggren et al. (1995) compilation.

Biostratigraphic event	Hole 980A	Hole 981A	Hole 982B	Hole 983A	Hole 984B	Berggren et al. (1995)
FO *E. huxleyi* (N)	0.31	0.34	0.18	0.26	0.28	0.26
LO *P. lacunosa* (N)	0.56	0.55	0.41	0.44	0.50	0.46
FO *Geophyrocapsa* spp. C/D (N)	0.80	0.73	0.82	0.65	0.68	
LO *Geophyrocapsa* spp. A/B (N)		1.23	1.00	1.25	1.28	
LO *H. selli* (N)		1.35		1.20		1.22
FO *P. doliolus* (D)		1.57				
LO *C. macintyrei* (N)		1.67	1.23	1.65		1.59
FO *Geophyrocapsa* spp. A/B (N)		1.70	1.60	1.70		
FO *Gr. inflata* (F)		2.14	2.08			2.09
LO *T. convexa* (D)		2.18				
LO *N. atlantica* (F)		2.35	2.30			2.41
LO *Gr. puncticulata* (F)		2.39	2.81			2.41
LO *D. surculus* (N)		2.66	2.65			2.55-2.59

Note: FO = first occurrence, LO = last occurrence, N = calcareous nannofossil event, F = planktonic foraminifer event, D = diatom event.